GLOBAL RAINBOW THERMOMETRY FOR AVERAGE TEMPERATURE MEASUREMENT OF SPRAY DROPLETS

J.P.A.J. van Beeck, D. Giannoulis, L. Zimmer and M.L. Riethmuller

von Karman Institute for Fluid Dynamics
Chaussée de Waterloo 72, B-1640 Rhode-Saint-Genèse, Belgium
(32) 2-359.96.11 (Phone) ; (32) 2-359.96.00 (Fax)

ABSTRACT

Global Rainbow Thermometry is presented. It is a new technique for measuring average size and temperature of spray droplets. For data inversion, a global rainbow pattern is employed, which is formed by constructive interference of laser-light scattering spherical droplets. The non-spherical droplets and liquid ligaments provide a uniform background and thus do not influence the interference pattern from which average size and temperature is derived. This is a large improvement with respect to standard rainbow thermometry, investigated since 1988, which is strongly influenced by particle shape. Moreover, the technique is applicable for smaller droplets than the standard technique because the global pattern is not spoiled by a ripple structure. Data inversion schemes based on inflection points, minima and maxima are discussed with respect to spray dispersion and droplet flux. The temperature derivation from inflection points appears to be independent of spray dispersion. Preliminary measurements in a water spray are reported. The mean diameter obtained from the rainbow pattern is smaller than the arithmetic mean diameter measured by phase-Doppler Anemometry. The accuracy of the temperature measurement by global rainbow thermometry is shown to be a few degrees Celsius.

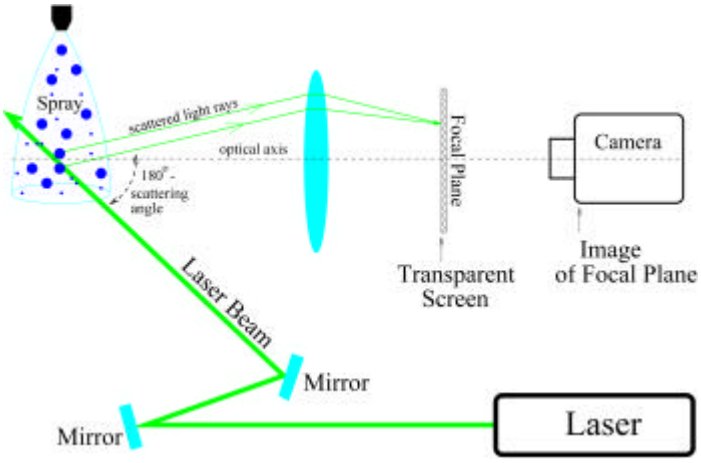

Fig. 1 Outline of the optical configuration for global rainbow thermometry. The global rainbow pattern is projected on the transparent screen that is filmed from the other side.

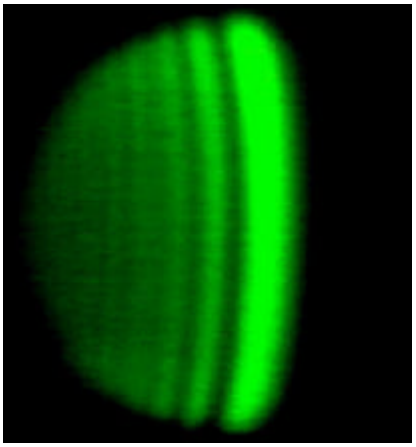

Fig. 2 A typical global rainbow pattern in a water spray recorded by a video camera.

1. STANDARD RAINBOW THERMOMETRY

Since several years, experimental results on standard rainbow thermometry have been reported by Roth et al. (1988, 1991), Sankar et al. (1993) and Van Beeck and Riethmuller (1994, 1995, 1996). Rainbow thermometry has already been applied with success to fuel combustion research by Sankar et al. (1996).

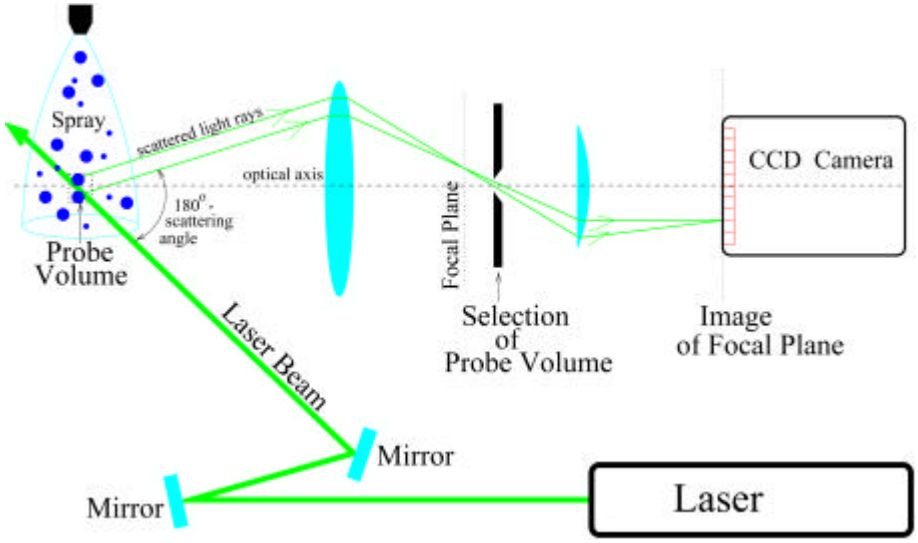

Fig. 3 Sketch of the set-up of standard rainbow thermometry. Remark the spatial filter that selects a probe volume containing a single droplet at a time.

Figure 3 sketches the optical layout. A laser, polarized perpendicularly to the scattering plane, illuminates a spray. The combination of a lens and a pinhole makes a spatial filter, selecting a probe volume through which one droplet passes at a time. A second lens projects the scattered light of this single particle on a CCD camera such that each pixel corresponds to a tiny range of scattering angles. In this way the primary rainbow from a single particle is recorded. This "rainbow" is of course monochromatic due to the use of a laser.

Figure 4 shows a typical rainbow pattern recorded by the set-up depicted in Figure 3. One can distinguish a low and a high-frequency interference structure, the Airy fringes (supernumerary bows) and the ripple structure, respectively. They are formed by optical interference between external and internal reflections of the laser beam by the droplet surface. Integration along the curvature of the fringes increases the signal to noise ratio (Giuliani et al. 1998), as can be seen in Figure 5.

From Figures 6 and 7, one can understand the reasoning for the data inversion scheme used for standard rainbow thermometry. Figure 6 depicts the dependency of the angular positions of the first five Airy fringes, q_1 to q_5, on the droplet temperature for constant diameter. For water, the rainbow pattern moves about 2.3° when the temperature changes 100°C. Remark that fringe spacing is independent of temperature. Subsequently, one can employ this spacing to obtain the droplet diameter without knowing the droplet temperature a priori. Figure 7 shows that the angular positions of the Airy fringes are indeed a function of diameter. For the determination of temperature and diameter, only the scattering angles for the first two maxima, q_1 and q_2, are employed. The rainbow angle, q_{rg}, derived from geometrical optics, is independent of the droplet dimension. Consequently, this angle is an indicator for the droplet temperature and thus and important parameter for the study on the rainbow technique.

To determine the extrema of the Airy fringes, one has to filter out the ripple structure (Fig.5). This interference structure gains importance for smaller droplets and thus influences the angular position of the Airy fringes, which renders the determination of the droplet temperature less accurate (Van Beeck 1997). For fuel droplets smaller than 30 μm, the accuracy of the temperature measurement by standard rainbow thermometry can therefore not be done better than about +/-6°C (Massoli 1998). In section 3, it will be shown that this problem does not exist for global rainbow thermometry.

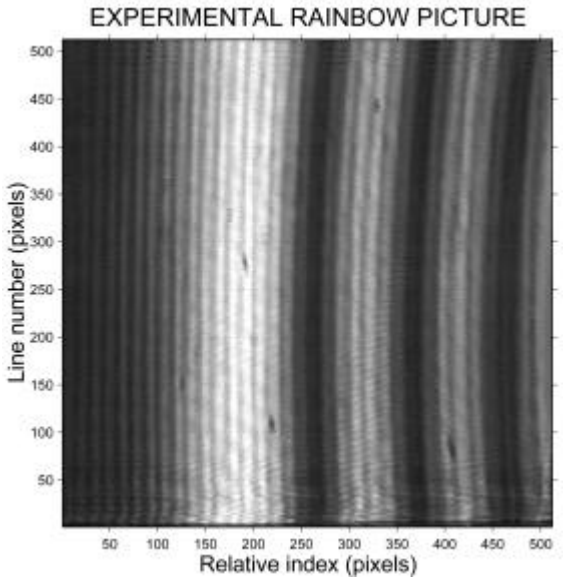

Fig. 4 A typical rainbow pattern coming from a single droplet in a water spray, recorded using the set-up of Fig 3. The horizontal axis is proportional to the scattering angle.

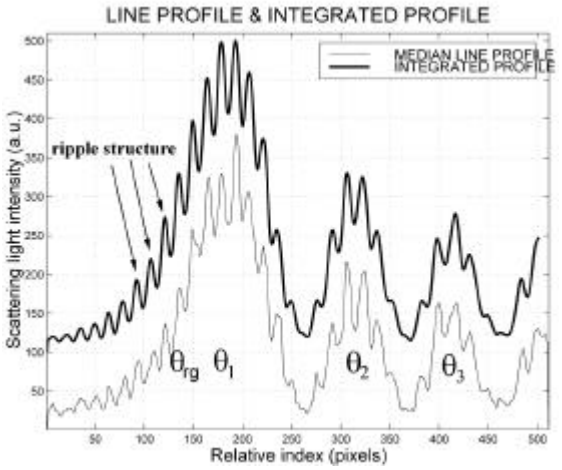

Fig. 5 The vertically-integrated profile of Fig. 4. The low-frequency pattern designates the supernumerary bows (Airy fringes) on top of which a ripple structure is superimposed.

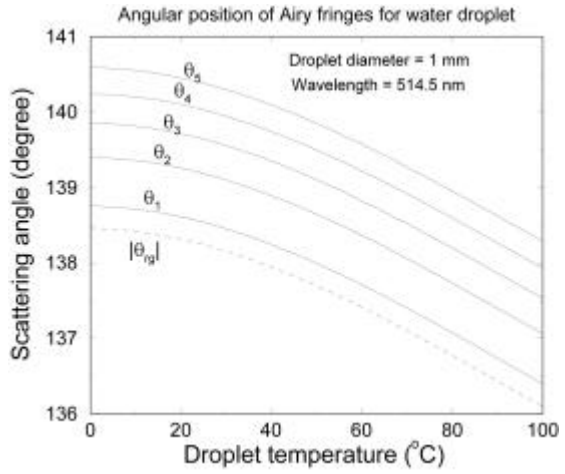

.

Fig. 6 Angular dependence of the first five Airy fringes on the droplet temperature for a fixed droplet diameter. Remark that fringe spacing is independent of droplet temperature. The Airy theory for the rainbow is utilized (Van Beeck 1997)

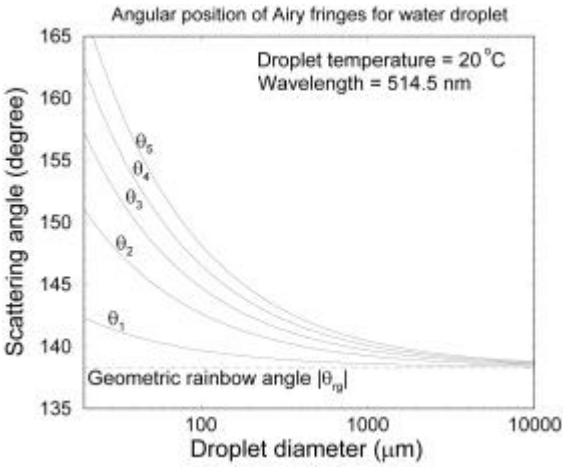

Fig. 7 Angular dependence of the first five Airy fringes as a function of droplet diameter for constant temperature.

2. DROPLET-SHAPE EFFECT ON ACCURACY OF STANDARD RAINBOW THERMOMETRY

There are several factors that can influence the accuracy of the rainbow technique. In the previous section the ripple structure was mentioned to spoil the temperature measurement for small droplets. Furthermore, temperature gradients inside the droplet also affect the temperature measurement (Anders et al. 1995, Corbin 1996 and Massoli 1998). However, the main source of measurement uncertainty for standard rainbow thermometry occurs for droplets that are non-spherical (Van Beeck and Riethmuller 1995, 1996, 1997). Take a look at Figure 8 to have an idea of the problem. It shows an interaction between the primary and secondary rainbow formed by a non-spherical droplet. It is clear that the position of the rainbow depends not only on the droplet temperature but also on its shape. This induces an ambiguity in the temperature measurement.

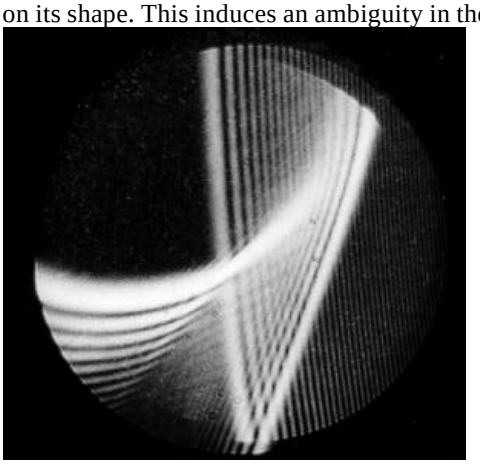

Fig. 8 A rainbow formed by a non-spherical droplet

From figures 9 and 10 one can estimate the influence of droplet shape on the geometrical rainbow angle q_{rg} (Moebius 1910). Moebius computed q_{rg} for an ellipsoid with respect to that of a sphere, for as long as the incident wave vector lies in the plane formed by two principal axes. The result is shown in Figure 10 as a function of the incidence angle Y and for different axis-ratios B/C. Close examination reveals that for a droplet non-sphericity of 1%, the rainbow pattern can change about 1^o. If one would be unaware of this shape-distortion, one can introduce a temperature error of 40^oC for water and about 20^oC for fuel. During the passed years, several algorithms for shape detection were proposed but neither of them could establish high confidence in the temperature measurement (Van Beeck and Riethmuller 1996, Sankar et al. 1996). This means that an error of $+/-40^oC$ or more is common for standard rainbow thermometry. Global rainbow thermometry solves this problem.

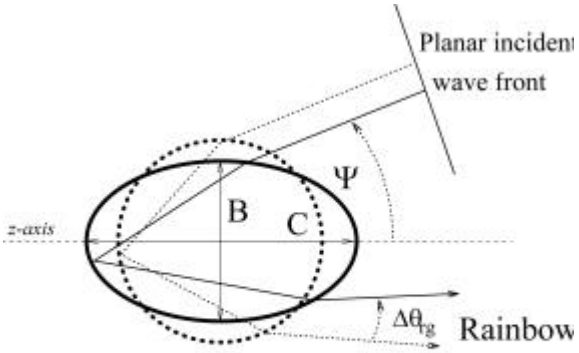

Fig. 9 Definition of parameters in the theoretical study of Moebius (1910) for the droplet-shape effect on the rainbow position.

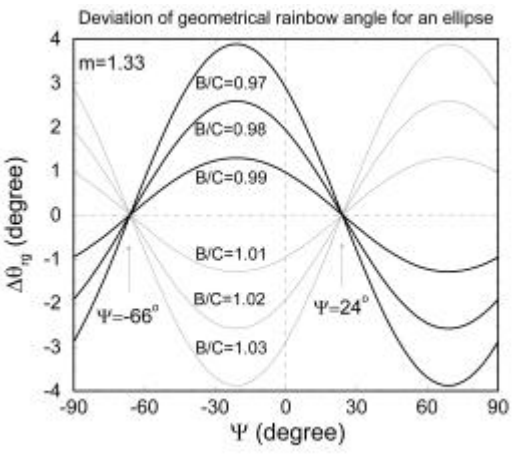

Fig. 10 Deviation of the geometrical rainbow angle q_{rg} as a function of Y (Figure 9) and axis ratio B/C.

3. PRINCIPLE OF GLOBAL RAINBOW THERMOMETRY

Global rainbow thermometry primarily aims at illuminating the non-sphericity effect that exists for the standard rainbow technique since its invention in 1988. The basic principles have been published by the authors in 1999.

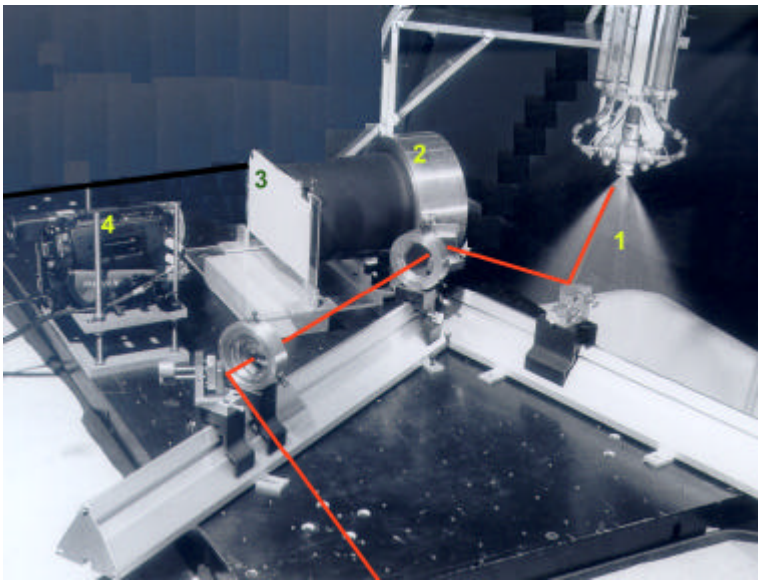

Fig. 11 Picture of the set-up, which was sketched in Fig. 1. One distinguishes the water spray (1), receiving lens (2), transparent screen (3) and the video camera (4). The laser beam is added during post-processing of the photograph and does not represent the real thickness.

Figure 11 shows a picture of the setup, sketched in Figure 1. A CW Argon-ion laser beam illuminates a water spray. The typical laser power is 100mW and the beam is expanded to a thickness of 15 mm. The most important remark is that there is no spatial filter like for standard rainbow thermometry (Figure 3). Instead, a transparent piece of paper is installed at the position of the focal plane of the receiving lens. This means that not one but all the droplets crossing the laser beam will contribute to the angular scattered light distribution, visible on the transparent screen. This results in the so-called global rainbow pattern that is recorded from the other side of the transparent screen by a digital video camera. The use of a transparent screen makes the alignment of the video camera to a minor issue. To calibrate the magnification factor of the camera, one records a millimeter paper image that is attached to the screen. Subsequently, the relationship between pixel number and the scattering angle is found via the focal length of the receiving lens.

A typical pattern is seen in Figure 2. It is recorded when the water spray works at stable ambient temperature. Horizontal profiles at different instants of time are plotted in Figure 12. Remark the stability of the Airy fringes. Although most probably numerous non-spherical droplets are crossing the laser beam, the position of the global rainbow pattern is not moving. This implies that the pattern is formed by constructive interference of the spherical droplets, because for each of them the geometrical rainbow angle is identical. Destructive interference occurs for the non-spherical droplets, because their interference fringes are randomly oriented and thus yield a uniform background. Consequently, there is no need for complex selection criteria to look for global rainbow patterns from spherical droplets. The selection is done automatically, just like the rainbow in the sky is a static phenomenon, even though numerous raindrops are not spherical.

Apart from the fact that the global pattern is formed by the spherical droplets only, it is interesting to notice that the visibility of Airy fringes is reduced with respect to rainbow signals like that of Figure 5. Moreover, the ripple structure is not visible at all. This makes the detection of the Airy maxima q_1 and q_2 easy, because only some noise needs to be filtered out. It has to be mentioned that the disappearance of the ripple structure has already been observed by Roth et al. (1991, 1992). These authors studied the average scattering diagram of a burning droplet stream with different droplet diameters. A size variation of less than

1µm made the ripple structure to vanish completely. However, the authors made no comments on the natural selection of spherical droplets by means of this averaged interference pattern.

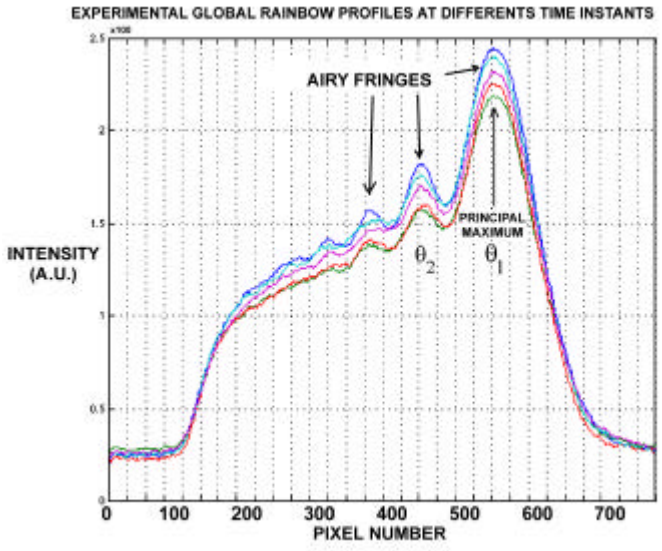

Fig. 12 Profiles of experimental global rainbow pattern at four different instants of time. Remark the stability of the pattern.

For the patterns of Figure 12 the mean diameter is 49µm +/- 3µm. This is computed from the fringe spacing q_2-q_1 as if the rainbow were formed by a single droplet. Phase-Doppler anemometry measures an arithmetic mean diameter of 60µm and a Sauter mean diameter of 130µm. From this, the question arises what mean diameter is deduced from the global rainbow pattern. This question is answered hereafter.

4. NUMERICAL SIMULATIONS OF THE GLOBAL RAINBOW PATTERN

To invert the global rainbow pattern to the mean droplet size and temperature, simulations of the pattern need to be performed. First results will be shown below for a spray with a statistically perfect log-normal droplet-size distribution at uniform temperature. The density function *f(d)* reads

$$f(d) = \frac{1}{sd\sqrt{2p}} \cdot e^{-\frac{1}{2}\left[\frac{\ln(d/d)}{s}\right]^2} \qquad (1)$$

The integral from zero to infinity over *f(d)* yields unity. *d* is a parameter representing the mean diameter of the spray and σ is the dispersion around it. Because there is a finite total number of droplets, N_{tot}, the distribution has to be discretized. With d_i-$Dd_i/2 < d < d_i$+$Dd_i/2$ being the diameter-range containing one droplet with diameter d_i, it follows

$$f(d_i)\Delta d_i = 1/N_{tot} \qquad (2)$$

Now, the arithmetic mean diameter D_{10} results in the following simple expression:

$$D_{10} = \sum_{i=1}^{N_{tot}} d_i f(d_i)\Delta d_i = \frac{1}{N_{tot}} \sum_{i=1}^{N_{tot}} d_i \qquad (3)$$

A similar simple expression is found for the commonly used Sauter mean diameter D_{32}:

$$D_{32} = \sum_{i=1}^{N_{tot}} d_i^{\,3} / \sum_{i=1}^{N_{tot}} d_i^{\,2} \qquad (4)$$

The influence of N_{tot}, s and d on the global rainbow pattern is investigated.

Figures 13 and 14 depict droplet-size distributions according to formula (1) for $s=0.2$ and $s=0.5$ respectively. Remark that for $s=0.5$ the distribution is less symmetric and ranges from 35µm to 280µm.

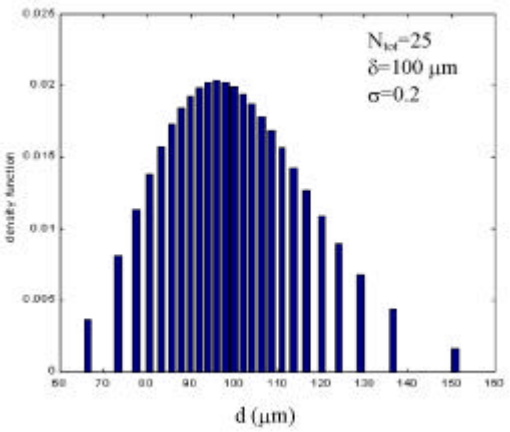

Fig. 13 Droplet size distribution for $s=0.2$.

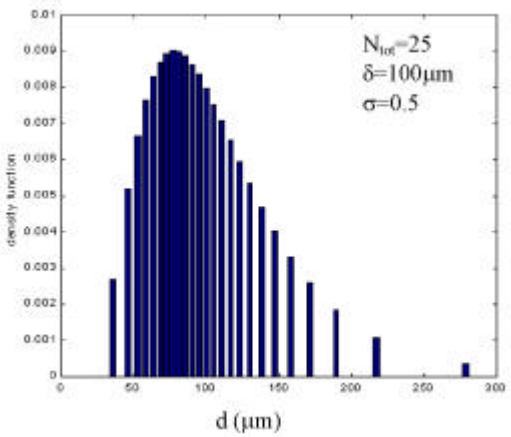

Fig. 14 Droplet size distribution for $s=0.5$.

To compute the scattering diagram of the global rainbow pattern, the scattered light intensity of each single droplet is summed, thereby neglecting optical interference between different droplets. The pattern for a single droplet is simulated using the normalized Airy function $Ai(x,d)$, with $x = q - q_{rg}$ (van Beeck 1997). Using this function implies that only the Airy fringes and no ripple structure is taken into account. The average scattered-light intensity distribution $Rnbw(x)$ becomes then

$$Rnbw(x) \propto \sum_{i=1}^{N_{tot}} Ai(x,d_i)^2 \cdot d_i^{7/3} \quad . \qquad (5)$$

The Airy function accounts for the normalized angular variation of the scattering diagram, whereas the factor $d_i^{7/3}$ describes the dependency of the scattered-light intensity on the droplet diameter within the primary rainbow region (Van de Hulst 1981). The distance droplet-receiver is the same for each droplet. Remind that the effect of droplet temperature and laser-light wavelength λ on the rainbow pattern lies in the geometrical rainbow angle q_{rg} (thus x). λ is set at 514.5nm for all the simulations in this paper.

Figure 15 shows normalized global rainbow patterns for s=0.2 and three different mean diameters d (Eq. 1). The total numbers of droplets N_{tot} is fixed at 100, which is sufficient to reach a converged solution. Note the perfect similarity between the curves.

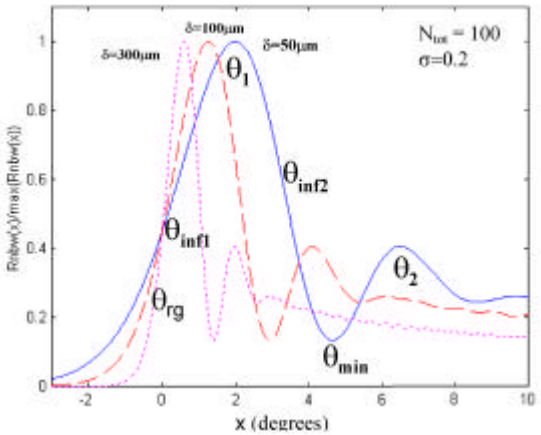

Fig. 15 Simulations of global rainbow patterns for different mean diameters at constant dispersion s. Furthermore, $x=q-q_{rg}$.

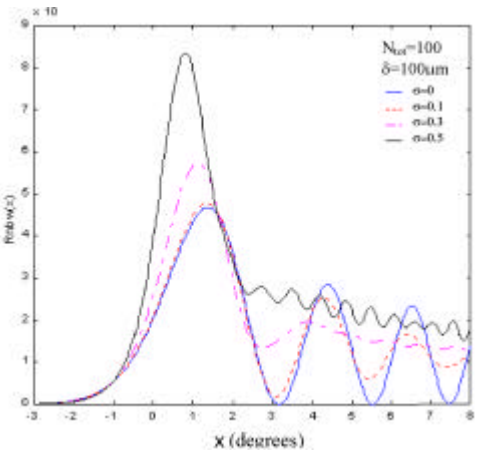

Fig. 16 Simulations of global rainbow patterns for different dispersions at constant mean diameter d. $x=q-q_{rg}$.

Figure 16 depicts global rainbow simulations for constant d, but with different dispersions s. Contrarily to Figure 15, the signals are not at all similar. The principal rainbow maximum tends to move towards the geometrical rainbow angle q_{rg} at $x = 0$, and the width of this maximum reduces with s. Moreover, the visibility of the fringes diminishes the higher the dispersion becomes. This influence on the visibility is more pronounced for higher x. This feature has also been observed in the experimental signal of Figure 12. However, complete resemblance between simulations and experiments has not been achieved. This could be due to the fact that

- the distance droplet-lens is neglected in the simulations. Looking to Figure 1, one understands that this distance depends on the position of the droplet in the laser beam.
- The contribution of nearly spherical droplets is not taken into account. It is likely that these droplets fill the "valleys" between the Airy maxima, thus reducing the fringe visibility.

5. DATA INVERSION ALGORITHMS FOR GLOBAL RAINBOW THERMOMETRY

Based on the simulations of the rainbow pattern (Section 4) one can evaluate what kind of diameter is obtained from the global rainbow. Three different algorithms are studied. They vary in the information taken from the signal. This can be the Airy maxima q_1 and q_2, the minimum q_{min} between both maxima, and the two inflection points q_{infl} and q_{inf2} around q_1 (see Figure 15).

The first algorithm is the existing one employed for standard rainbow thermometry. The droplet diameter, D_{Airy}, is derived from the distance between the first two Airy fringes, q_1 and q_2, using the Airy theory for the rainbow (Van Beeck and Riethmuller 1995,1997, Sankar et al. 1996),

$$D_{Airy} = 1016.2\, l\, (q_2 - q_1)^{-3/2}, \qquad (6)$$

valid for a refractive index $m=4/3$. Once D_{Airy} is known, the temperature is computed from the geometrical rainbow angle, deduced from q_1 and D_{Airy} (van Beeck 1995, 1997),

$$q_{rg} = q_1 - 46.18(l / D_{Airy})^{2/3}, \qquad (7)$$

where the second term on the right hand side is valid for $m=4/3$**.** The relationship between q_{rg} and the temperature has been drawn for water in Figure 6.

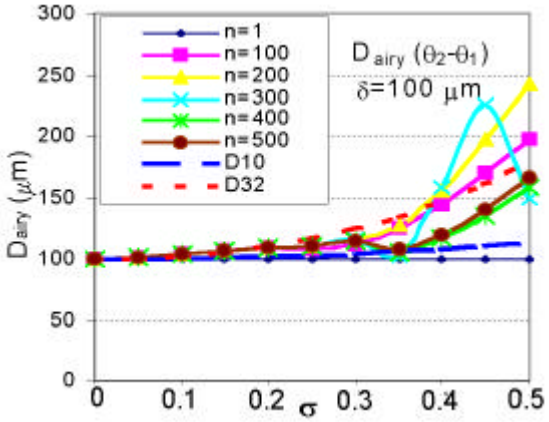

Fig. 17: The Airy diameter, computed from q_2-q_1 as a function of the spray dispersion s for various amounts of droplets (Eq. 6).

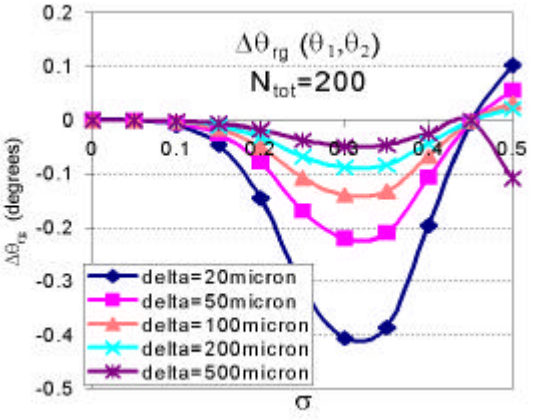

Fig. 18: The deviation of q_{rg}, based on the first two Airy maxima, from its value at $s=0$, as a function of s and different mean diameters d (Eq. 7).

Figure 17 shows D_{Airy} as a function of s for $d=100mm$ and different amounts of droplets. Until $s=0.3$, D_{Airy} equals the Sauter mean diameter D_{32}. For higher s, the Airy diameter depends on the total number of droplets forming the global rainbow. This number is unknown in the experiments; hence Eq. (6) becomes useless for $s>0.3$. Figure 18 depicts the results of Eq. (7) for different d with $N_{tot}=200$. The deviation of q_{rg} from its value at $s=0$ reaches –0.4° for a diameter of 20µm, which corresponds to an

uncertainty in the temperature measurement of about 16°C for water. Consequently, the algorithm employed for standard rainbow cannot be applied for a poly-dispersed spray to compute the average droplet size and temperature, especially when the mean droplet diameter is smaller than 100μm. The problem with this algorithm is related to the fact that the second Airy fringe disappears for large σ (see Figure 16).

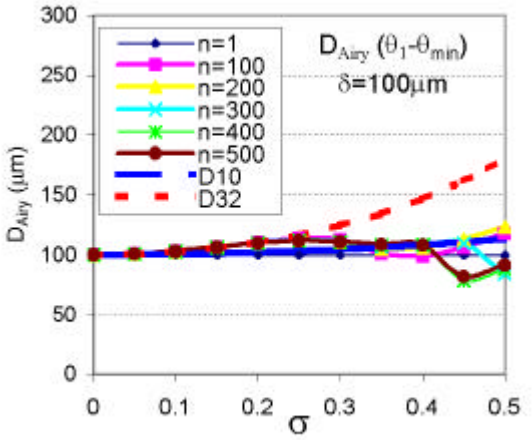

Fig. 19: The Airy diameter, computed from q_1-q_{min}, as a function of the spray dispersion s for various amounts of droplets (Eq. 8).

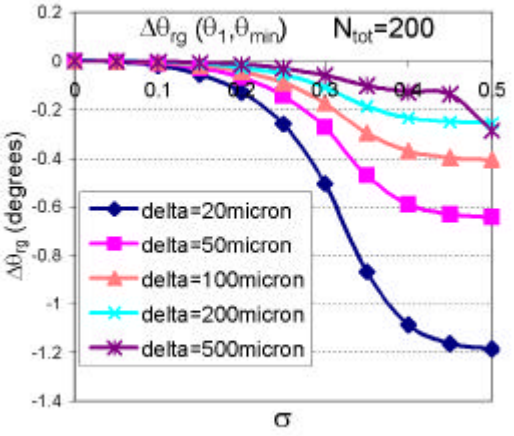

Fig. 20: The deviation of q_{rg}, based on q_1 and q_{min}, from its value at s=0, as a function of s for different mean diameters d (Eq. 9).

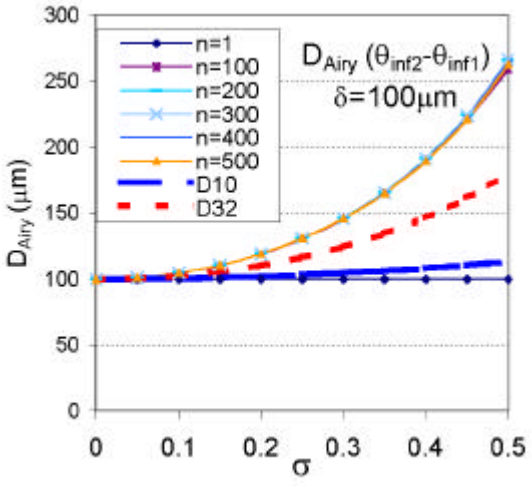

Fig. 21: The Airy diameter, computed from q_{inf2}-q_{inf1}, as a function of the spray dispersion s for various amounts of droplets (Eq. 10).

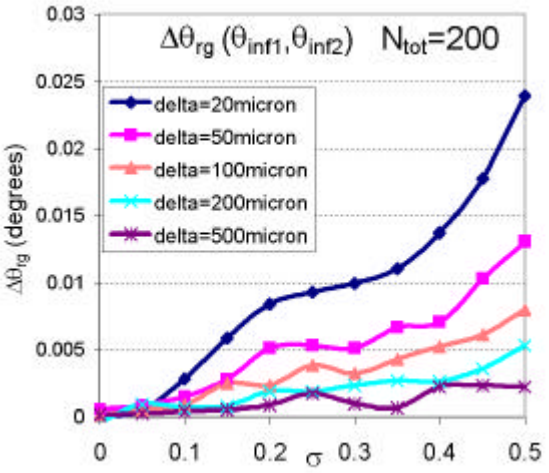

Fig. 22: The deviation of q_{rg}, based on q_{inf2} and q_{inf1}, from its value at s=0, as a function of s for different mean diameters d (Eq. 11).

The second algorithm employs the maximum of the principal Airy fringe q_1 and the first minimum q_{min} (Figure 15). From these parameters one can deduce D_{Airy} and q_{rg} using the Airy theory for the rainbow (e.g. Van Beeck 1997):

$$D_{Airy} = 462.6\, l\, (q_{\min} - q_1)^{-3/2}, \qquad (8)$$

$$q_{rg} = q_1 - 46.18(l / D_{Airy})^{2/3}. \qquad (9)$$

Figures 19 and 20 depict D_{Airy} and Dq_{rg}, respectively. There is no improvement in the temperature measurement (Figure 20) with respect to the algorithm based on q_1 and q_2. However, concerning the droplet-size measurement (Figure 19), D_{Airy} follows D_{32} up to $s=0.25$. For $0.25<s<0.4$, D_{Airy} is closer to the arithmetic mean diameter D_{10}. For even larger s, D_{Airy} weakly depends on N_{tot}. The same behavior is found for other d, because the rainbow signals are similar (Figure 15).

The most interesting results are obtained for the data inversion algorithm based on the deflection points around q_1, i.e. q_{infl} and q_{inf2} (Figure 15). The relationship between these points and D_{Airy} and q_{rg} reads:

$$D_{Airy} = 531.6\, l\, (q_{\inf 2} - q_{\inf 1})^{-3/2}, \qquad (10)$$

$$q_{rg} = q_{\inf 1} - 13.91(l / D_{Airy})^{2/3}. \qquad (11)$$

Roth et al. (1996) already noted that q_{infl} lies very close to the geometrical rainbow angle q_{rg}, thus being a good indicator for the droplet temperature. Figure 21 shows that D_{Airy} is independent of N_{tot} up to $s=0.5$, but it exceeds the Sauter mean diameter D_{32} considerably. This is related to the decrease of the width of the principal rainbow maximum when s increases (Figure 16). But look to Figure 22! Dq_{rg} is never larger than 0.025°, which means that this algorithm ensures and uncertainty in the temperature measurement of less than 1°C.

Finally, it is interesting to mention that the spray-dispersion s correlates with the ratio of D_{Airy} from the inflection points and the one derived from q_1 and q_{min}, as is seen in Figure 23. The resulting curve can therefore be used to determine the width of the droplet size distribution. Unfortunately, for $s>0.4$, the relationship depends also on the total number of droplets N_{tot}.

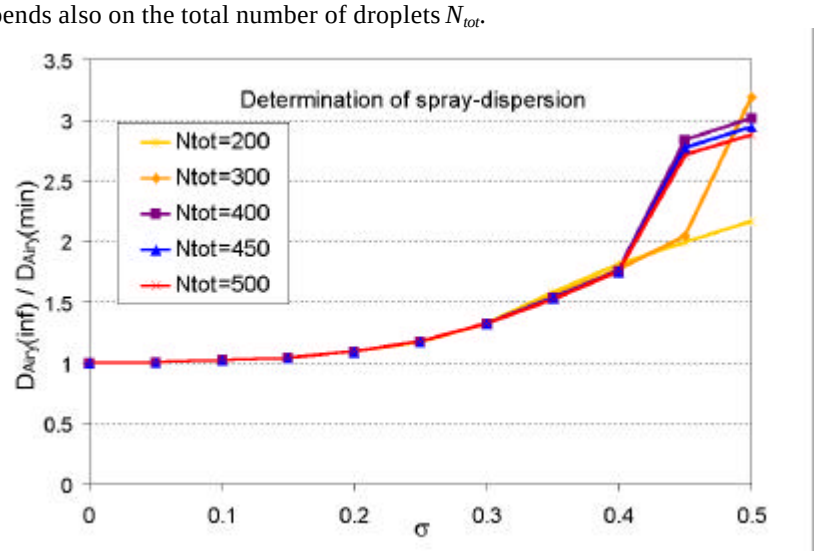

Fig. 23: The ratio between the droplet diameter derived from the inflection points and the one derived from the first Airy maximum and minimum is plotted as a function of the non-dimensional width of the droplet size distribution.

6. EXPERIMENTAL RESULTS

Above-mentioned data inversion schemes have been applied to the experimental signals of Figure 12. D_{Airy}, based on the first Airy maximum and minimum (Eq. 8), yields 48µm, but from the inflection points (Eq. 10) a mean droplet diameter of 56µm is obtained. The precision in these diameters is about 5%, hence the curve in Figure 23 yields a s between 0.2 and 0.3. For this spray-dispersion, the diameter 48µm should be close to D_{32}, but phase-Doppler anemometry (PDA) gives 130µm. This large discrepancy could be explained by the fact that the rainbow method is much more sensitive to droplet shape than PDA (Tropea 1999). PDA measures a mean Sauter diameter of the spherical and spheroidal droplets. On the other hand, the global rainbow pattern is formed by the most spherical droplets only, thus the smaller ones. This leads to a mean Sauter diameter for the rainbow technique that is inferior to that of PDA.

All simulations in the previous section are made at constant temperature. The whole picture could change when the global rainbow is formed by droplets with different temperatures. Nevertheless, it is interesting to see what the technique gives so far. Temperature measurements are presented in Figure 24. It shows the droplet temperature in the water spray of Figure 11 at a distance of 10cm from the spray nozzle. The initial nozzle temperature has been monitored by a thermocouple and has been varied between 19°C and 68°C. The ambient temperature is 21°C. The method of the inflection points is used (Eq. 11). Each rainbow temperature is obtained after averaging 50 video images, taken at different instants of time. This ensures convergence of the mean temperature measurement with respect to the number of droplets forming the rainbow. Although the precision seems to be less than 1°C, the tendency is correct. The spray droplets cool down.

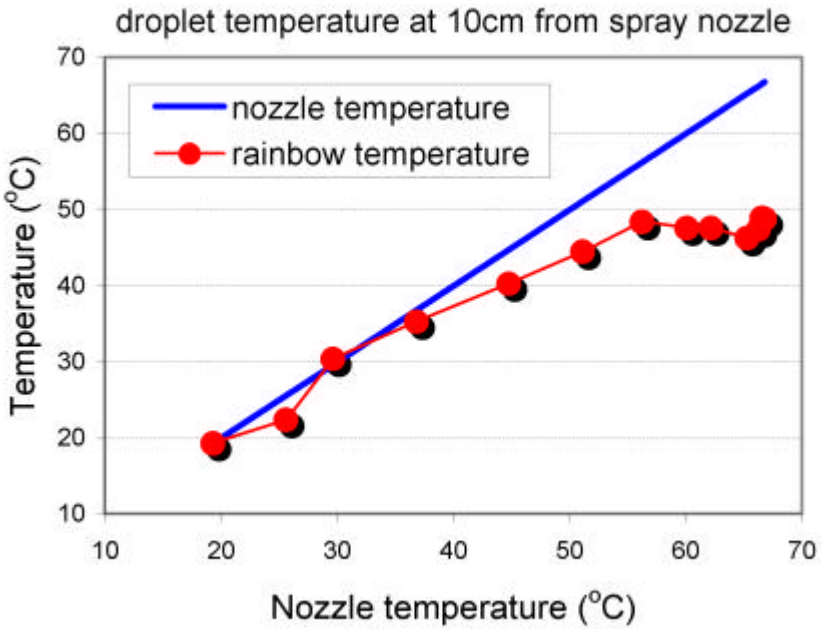

Fig. 24: Rainbow temperature in a water spray at 10cm from the injection point as a function of the injection point temperature.

7. CONCLUSIONS

Experimental and numerical results on global rainbow thermometry have been reported and compared to the standard rainbow technique. Low CW laser power is needed to create an average, so-called global, rainbow pattern. This pattern is formed by all the spherical droplets that cross the laser beam during the integration time of the video camera. The non-spherical particles are supposed to create a uniform background. Because the selection of spherical droplets happens naturally, the destructive influence of droplet shape on the accuracy of the temperature measurements is overcome. Moreover, the pattern is smooth and not spoiled by an additional ripple structure that would deteriorate the temperature derivation from the global rainbow pattern.

Simulations of the global rainbow pattern have been performed using the Airy function and a log-normal distribution for the spray droplet diameters. All droplets are supposed to be at the same temperature and at the same distance from the detector. The simulations show that there exists a similitude for global rainbow patterns of different mean droplet diameters. However, for increasing spray-dispersion, the similitude does not hold because signal visibility reduces significantly. Moreover, the larger the spray dispersion, the more droplets are needed to reach a converged solution. An important result is that the principal rainbow maximum, from which the mean temperature is derived, becomes narrower for increasing width of the droplet size distribution. This renders the detection of the rainbow displacement, thus temperature measurement, more accurate.

Three data-inversion algorithms have been investigated. The standard algorithm, based on the two important interference maxima, fails for a poly-dispersed spray because the lower maximum vanishes. The second algorithm derives the mean droplet size and temperature from the first maximum and first minimum. A mean diameter is obtained somewhere between the arithmetic and Sauter mean diameter, but the temperature measurement is not reliable. A correct temperature is derived from the third algorithm, employing the inflection points around the principal rainbow maximum. For this algorithm, the uncertainty is always less than 1°C. The mean droplet diameter obtained from this method is much larger than the Sauter diameter. That is why the ratio between this diameter and the one derived from the first maximum and minimum can give an idea about the spray dispersion.

Resemblance between experimental rainbow patterns and the simulations is not perfect as far as relative peak intensities are concerned. One reason could be the influence of nearly spherical droplets, which is neglected in the simulations. Nevertheless, rainbow temperatures have been measured with success in a heated water spray. The precision is a few degrees Celsius. The mean droplet diameter, measured by the rainbow method, appears to be considerably smaller than the one obtained by phase-Doppler anemometry. This is probably because global rainbow thermometry only sees the smaller, most spherical droplets.

ACKNOWLEDGMENTS

The authors thank M. Santonastasi and J. Sanz for their contribution to the paper.

REFERENCES

N. Roth, K. Anders, and A. Frohn 1988, Simultaneous measurement of temperature and size of droplet in the micrometer range, 7th International Congress on Optical Methods in Flow and Particle Diagnostics ICALEO 88, L.I.A. (Sunnyvale U.S.A.), vol. 67, pp. 294-304.

N. Roth, K. Anders, and A. Frohn 1991, Refractive-index measurements for the correction of particle sizing methods, Applied Optics, vol. 30, no. 33, pp. 4960-4965.

S.V. Sankar, K.H. Ibrahim, D.H. Buermann, M.J. Fidrich, and W.D. Bachalo 1993, An integrated phase doppler/rainbow refractometer system for simultaneous measurement of droplet size, velocity, and refractive index, The 3rd International Congress on Optical Particle Sizing (Yohokama, Japan), August 1993, pp. 275-284.

J.P.A.J van Beeck and M.L Riethmuller 1994, Simultaneous determination of temperature and size of droplets from the rainbow using Airy theory, Proc. of the 7th International Symposium on Applications of Laser Techniques to Fluid Mechanics (Lisbon, Portugal), vol. 2, pp. 21.5.1-21.5.6., also in "Developments in Laser Techniques and Applications to Fluid Mechanics", R.J. Adrian et al. (eds.), Springer, pp. 330-339.

J.P.A.J. van Beeck and M.L. Riethmuller 1995, Nonintrusive measurements of temperature and size of single falling raindrops, Applied Optics, Vol. 34, No. 10, pp. 1633-1639.

J.P.A.J. van Beeck and M.L. Riethmuller 1996, Rainbow phenomena applied to the measurement of droplet size and velocity and to the detection of nonsphericity, Applied Optics, Vol. 35, No. 13, pp. 2259-2266.

S.V Sankar, D.H. Buermann, and W.D. Bachalo 1996, An advanced rainbow signal processor for improved accuracy in droplet temperature measurements, Proc. of the 8th International Symposium on Applications of Laser Techniques to Fluid Mechanics (Lisbon, Portugal) vol. 1, pp. 9.3.1.-9.3.9.

F.L.M. Giuliani, J.P.A.J. van Beeck and M.L. Riethmuller 1998, Thermométrie par Arc-en-ciel: Technique d'acquisition de donnée à l'aide d'un laser Nd:YAG et traitement de signaux 2D, in Recueil des Actes du 6e Congrès Francophone de Vélocimétrie Laser, ISL Saint-Louis, France, pp. B3.1-B3.6.

J.P.A.J. van Beeck 1997, Rainbow Phenomena: development of a laser-based, non-intrusive technique for measuring droplet size, temperature and velocity, Ph.D-thesis, Eindhoven University of Technology, ISBN 90-386-0557-9.

P. Massoli 1998, Rainbow refractometry applied to radially inhomogeneous spheres: the critical case of evaporating droplets, Applied Optics, Vol. 37, No. 15, pp 3227-3234.

K. Anders, N. Roth, and F. Frohn 1995, Theoretical and experimental studies of the influence of internal temperature gradients on rainbow refractometry, Proc. of the 4th International Congress on Optical Particle Sizing (PARTEC), Nuernberg, Germany, 1995, pp. 419-428.

F. Corbin, A. Garo, G. Gouesbet, and G. Gréhan 1996, Réfractométrie d'arc-en-ciel: Application au diagnostic des gouttes avec gradient d'indice, in Recueil des Actes du 5e Congrès Francophone de Vélocimétrie Laser, Université et Institut des Sciences Appliquées de Rouen, URA CNRS 230/CORIA, Rouen, France, pp. E1.1-E1.8.

W. Moebius 1910, Zur Theorie des Regenbogens und ihrer experimentellen Prüfung, Ann. Phys. (Leipzig), 33, pp 1493-1558.

J.P.A.J. van Beeck, D. Giannoulis, L. Zimmer, and M.L. Riethmuller 1999, Global rainbow thermometry for droplet-temperature measurement, Optics Letters, Vol. 24, No. 23. pp. 1696-1698.

N. Roth, K. Anders, and A. Frohn 1992, Simultaneous determination of refractive index and droplet size using Mie theory, Proc. of the 6th International Symposium on Applications of Laser Techniques to Fluid Mechanics (Lisbon, Portugal), Vol 1, pp. 15.5.1-15.5.5.

H.C. van de Hulst 1981, Light scattering by small particles, Dover Publications, Inc., New York, ISBN 0-486-64228, pp 243-246

N. Roth, K. Anders, and A. Frohn 1996, Size insensitive rainbow refractometry: theoretical aspects, Proc. of the 8th International Symposium on Applications of Laser Techniques to Fluid Mechanics (Lisbon, Portugal), Vol 1, pp. 9.2.1-9.2.6.

C. Tropea 1999, Developments of specialized phase-Doppler techniques and refractive index measurements, Lecture Series on Optical Diagnostics of Particles and Droplets, von Karman Institute, Sint-Genesius-Rode, Belgium.